Biosensors and Bioelectronics 155 (2020) 112113

Contents lists available at ScienceDirect

Biosensors and Bioelectronics

journal homepage: http://www.elsevier.com/locate/bios

Capillary-assisted microfluidic biosensing platform captures single cell secretion dynamics in nanoliter compartments

Amin Hassanzadeh-Barforoushi [a,b,c,d,*], Majid Ebrahimi Warkiani [e,f], David Gallego-Ortega [b,g], Guozhen Liu [c,d], Tracie Barber [a]

[a] School of Mechanical and Manufacturing Engineering, University of New South Wales, Sydney, NSW, 2052, Australia
[b] Cancer Division, Garvan Institute of Medical Research/ the Kinghorn Cancer Centre, Sydney, NSW, 2010, Australia
[c] Graduate School of Biomedical Engineering, ARC Centre of Excellence in Nanoscale BioPhotonics (CNBP), Faculty of Engineering, University of New South Wales, Sydney, NSW, 2052, Australia
[d] Australian Centre for NanoMedicine, University of New South Wales, Sydney, 2052, Australia
[e] School of Biomedical Engineering and Institute for Biomedical Materials & Devices (IBMD), University of Technology Sydney, Sydney, NSW, 2007, Australia
[f] Institute of Molecular Medicine, Sechenov First Moscow State Medical University, Moscow, Russia
[g] St Vincent's Clinical School, Faculty of Medicine, University of New South Wales, Sydney, NSW, 2052, Australia

ARTICLE INFO

Keywords:
Single cell analysis
Cancer
Cellular heterogeneity
Dynamic protease secretion
Biosensing
Capillary microfluidics

ABSTRACT

Cancer cells continuously secrete inflammatory biomolecules which play significant roles in disease progression and tumor metastasis toward secondary sites. Despite recent efforts to capture cancer cells' intercellular secretion heterogeneity using microfluidics, the challenges in operation of these systems as well as the complexity of designing a biosensing assay for long-term and real-time measurement of single cell secretions have become grand research barriers. Here, we present a new capillary-based microfluidic biosensing approach to easily and reliably capture ~500 single cells inside isolated dead-end nanoliter compartments using simple pipette injection, and quantify their individual secretion dynamics at the single cell resolution over a long period of culture (~16 h). We first present a detailed investigation of the fluid mechanics underlying the formation of nanoliter compartments in the microfluidic system. Based on the measurement of single cell capture efficiency, we employ a one-step FRET-based biosensor which monitors the single cancer cells' protease activity. The sensor reports the fluorescent signal as a product of amino acid chain cleavage and reduction in its quenching capability. Using the single cell protease secretion data, we identified modes of cell secretion dynamics in our cell sample. While most of the cells had low secretion levels, two other smaller and more aggressive secretion dynamics were cells with secretion modes that include sharp spikes or slow but progressive trend. The method presented here overcomes the difficulties associated with performing single cell secretion assays, enabling a feasible and reliable technique for high throughput measurement of metabolic activities in cancer cells.

1. Introduction

Cellular heterogeneity is playing a critical role in driving and regulating processes in human organs as in chemotherapeutic drug response (Stevens et al., 2016), neural systems behavior (Stefen et al., 2018), immune response (Satija and Shalek, 2014), organ regeneration (Hassanzadeh-Barforoushi et al., 2016) and embryonic development (Krieger and Simons, 2015). Over the past decade, single cell analysis tools have been introduced to measure a wide range of heterogeneous factors such as genomic (Shendure et al., 2017), transcriptomic (Pickrell et al., 2010), and proteomic (Wu and Singh, 2012) variations. Despite extensive efforts in obtaining data from single cells using technologies such as Fluorescence-activated cell sorting- FACS (Atkin-Smith et al., 2017), SCI-seq (Vitak et al., 2017), and Drop-seq (Macosko et al., 2015), none of those methods are able to quantify critical dynamic phenomena such as single cell protein secretion and metabolic activity. Such information is invaluable for unraveling mechanisms controlling the single cells' sensing, decision making and signaling (Konry et al., 2016).

Real-time monitoring of the single cell dynamics requires identification of the target analyte, design of an appropriate biosensor, and finally employment of a suitable signal read-out method (Jeknić et al., 2019). Single cell intracellular dynamics have been quantified by

* Corresponding author. Postdoctoral Research Fellow, UNSW, Australia.
E-mail addresses: a.hasanzadeh.ut@gmail.com, a.hassanzadehbarforoushi@unsw.edu.au (A. Hassanzadeh-Barforoushi).

https://doi.org/10.1016/j.bios.2020.112113
Received 2 November 2019; Received in revised form 6 February 2020; Accepted 18 February 2020
Available online 19 February 2020

targeting biomolecules such as transcription factors (Tay et al., 2010), metabolic byproducts (Li et al., 2019) and second messengers (Colombo et al., 2017) using fluorescent fusion proteins, fluorescent bio-probes and Fluorescence Resonance Energy Transfer (FRET) probes, respectively. Measurement of these intracellular signals is relatively easy as the cell membrane keeps proteins inside the cell with the concentration in a well-detectable range (Lo et al., 2015).

Unlike intracellular events, extracellular secretion is diffused into the cell's surrounding environment, diluted by the media and therefore yields significantly lower concentrations. Measuring such events necessitates cell encapsulation to preserve the secreted molecules and requires incorporation of more sensitive biosensors. Sandwich immunoassays with capture antibody coated on microwells (Shirasaki et al., 2014) or co-encapsulated microspheres (Konry et al., 2011; Chokkalingam et al., 2013) and capture technology on cell membrane (Liu et al., 2019) have been introduced to measure pg/ml of cytokine secretion from single cells. In a new effort, the sandwich assay has also been used for multiplexed single cell secretion using antibody barcode patterning in a nanoliter microtrough array (Chen et al., 2019) and measuring secretion frequency and magnitude through quantitative microengraving technique (Han et al., 2010). While the well-known mechanism of sandwich assay makes it a desirable technique, the binding nature of the assay, its incapability to perform continuous measurement and its reliance on the antibody specificity limits the rate of the measurement and its robustness. To overcome these challenges, label-free methods based on mass spectrometry (Amantonico et al., 2010), electrochemistry (Zhou et al., 2013) and optical biosensing (Li et al., 2018) have been developed. However, the level of complexity associated with these assays as well as their low throughput compromises their widespread adoption. Methods based on one step chemical reaction of the target analytes and recognition molecules are simple, eliminate complicated surface functionalization steps, and are capable of continuous measurement of cell secretion dynamics (Cao et al., 2018; Zhang et al., 2019). For instance, protease activity of single circulating tumor cells (CTCs) (Dhar et al., 2018) and human leukemia cell lines (Haaβ et al., 2015) were quantified using peptide cleavage and uptake by the single cells.

In order to maintain single cells' chemical signature and achieve the level of sensitivity required for low concentration of extracellular secretion, microfluidic methods based on cell encapsulation in microchambers (Eyer et al., 2012; Shen et al., 2015) and pico/nanoliter droplets (J. Collins et al., 2015; Köster et al., 2008) have been proposed. However, both methods entail complex fluidic control such as multilayer valving system (Dang et al., 2019), challenging pressure adjustment for tuning droplet size and droplet immobilization (Courtney et al., 2017). To address these issues, methods for simultaneous generation and immobilization of single cell compartments in the form of semi-droplets have been introduced (Cohen et al., 2010; Hassanzadeh-Barforoushi et al., 2018; Sposito and DeVoe, 2017). Sample digitization into an array of dead-end traps was achieved using geometrical pinning of the liquid sample (Cohen et al., 2010; Sposito and DeVoe, 2017). While providing a self-filling capability, the digitization mechanism works only within a narrow range of geometrical and fluidic properties. Another concern about digitization systems is the formation of trapped air bubbles. This issue has been addressed by designing air vents (Shemesh et al., 2014) or air plugs (Hassanzadeh-Barforoushi et al., 2018) at the end of each trap. Despite operational simplicity offered by such strategy the underlying mechanism governing the air venting and the fluid mechanics of the simultaneous generation and splitting of droplet compartments in those systems remains unanswered.

In this paper, we present a detailed analysis of the engineering of a microfluidic device for the formation of an array of hundreds of bubble-free nanoliter liquid compartments. This analysis provides a deep insight for designing microfluidic systems for long-term single cell encapsulation and real-time secretion profiling. In addition, by incorporating capillary forces, the presented approach offers simplicity and reliability of performing single cell secretion assays. Once single cell encapsulation is achieved, we explore opportunities for performing single cell secretion profiling. We report the rate at which single cells of the same phenotype produce proteases and describe different modes of cell secretion dynamics.

2. Materials and methods

2.1. Design and fabrication procedure

Channel designs were drawn in AutoCAD 2015 (Autodesk®) and printed on a high resolution glass photomask. Photolithography using a Karl Suss MA6 Mask Aligner (SUSS MicroTec, Germany) was then used to reflect the mask pattern on an nLOF2020 coated silicon on insulator (SOI) wafer (100 mm wafer diameter, 80 ± 1 μm top layer, 2 μm buried oxide layer, and 500 ± 15 μm base silicon layer). Deep Reactive Ion Etching (DRIE) using STS system was employed to make the final high aspect ratio (1:8) device. Fig. S1 demonstrates the complete procedure for the mold fabrication. Fabrication of the PDMS chips was performed via soft lithography on the SOI wafer. Briefly, the wafer surface was coated with Methyltrichlorosilane (Sigma, USA) via vapor deposition. PDMS (Sylgard 184, Dow Corning, USA) pre-polymer (1:10 base to curing agent ratio) was fully degassed, poured on the wafer and baked in the oven for 3 h at 100 °C. The hardened PDMS was then cut from the mold and access holes were punched using 1.5 mm biopsy punch. The devices were then bonded to the glass substrate through plasma bonding to close the channels.

2.2. Cell culture

Breast cancer cell line MDA-MB-231(ATCC® HTB-26™) was cultured in RPMI medium (Gibco, 11,875) with seeding density of 10^4 cells/cm^2 using a T-75 flask together with 10% FBS, 1% penicillin/streptomycin, and 6% insulin and passaged when 80% confluent.

2.3. Microfluidic cell culture and cell encapsulation

A 80% confluent flask of MDA-MB-231 cancer cells was trypsinized to achieve separated single cells in medium. Cell viability (>90%) and concentration was obtained using a Countess automated cell counter (Invitrogen). To investigate the optimal concentration which gives the highest single cell occupancy in the device, a wide range of cell solution concentrations were made from the concentrated cell sample. Microfluidic devices were loaded with cell solutions comparable to their volume (≈ 10 μl) and preserved in a humidity chamber. Cell viability in the device was monitored every 12 h using a Leica DM 4000 light microscope (Wetzlar, Germany).

2.4. Cell loading in the device

In order to inject the cell samples in the device, 10 μl of the cell solution with predefined cell density is taken by a handheld pipette which is then placed at the inlet port of the device. The cells were then injected in and filled the device simply by dispensing the sample from the pipette into the device. In the next step, a pipette with no sample is placed at the inlet port and is pushed to force the air flow into the channel and form the droplet compartments. The residual sample is then collected in the outlet port. Finally, FC-oil is taken by the pipette and injected through the inlet port to sheath the droplets.

2.5. Real-time single cell secretion profiling assay

The cell solution with two times concentration for maximum single cell occupancy and the FRET-based polypeptide Matrix Metalloproteinase (MMP) substrate PEPDAB008 (Biozyme, Apex, NC, USA) were mixed in a 1:1 ratio and then loaded into the device using pipette

injection. The final concentration of MMP substrate was adjusted to 40 μM in 50 mM Tris buffer (150 mM NaCl, 2 mM $CaCl_2$, 5 μM $ZnSO_4$, and 0.01% Brij-35; PH 7.5). Real-time measurement of single cell secretion was achieved with the optimal exposure time of 200 ms using a Leica DMi8 live cell imaging inverted microscope.

2.6. Numerical simulation

In order to understand the behavior of the flow and interface movement (along the microfluidic trapping array facing the expansion and contraction geometries), a series of numerical simulations based on finite element analysis of the two-phase fluid flow in microfluidic systems (Nejat et al., 2014; Rafeie et al., 2017) were performed using COMSOL multiphysics software. The "Laminar Two-Phase Flow- Phase Field" was chosen as the physics with the Transient Phase Initialization as the solver mode. In order to define the initial location of the liquid-air interface, the geometry of the channel was designed by unifying two subsections at the opposite sides of the initial interface. Pressure boundary condition of 1300 Pa and 0 Pa was set at the inlet and outlet respectively. The boundary condition at the walls was set to wetted wall boundary condition with the contact angle of $107^\circ = 1.8679$ radian for PDMS channels (Ismail et al., 2009). A triangular mesh was used to grid the fluid domain and mesh independency was ensured by plotting the maximum velocity versus the number of mesh elements (Fig. S2). In setting up the time-dependent solver the time span/step which captures the total period of interface movement were chosen. Fluid properties for water and air were set to the densities of $\rho_{water} = 998$ kg/m3 and $\rho_{air} = 1.1614$ kg/m^3, dynamic viscosities of $\mu_{water} = 1.002 \times 10^{-3}$ kg/m.s and $\mu_{air} = 1.846 \times 10^{-5}$ kg/m.s and surface tension of $\gamma = 0.0728$ N/m.

2.7. Image and data analysis

Images obtained from microscopy of the entire device were used to determine the cell occupancy and co-trapping occupancy in the trap array and were triplicated for each concentration to ensure statistical significance. All other experiments throughout the paper including the comparison between two groups were at least triplicated and the statistical significances were examined using student's T-test. In order to analyze the gradient steepness, the mean grey intensity of the food dye in different rows was calculated using ImageJ software. Finally, quantification of the single cell secretion over time has been performed by defining a region of interest (ROI) of all of the liquid compartments using ImageJ and measuring the mean grey value for those areas over time.

3. Results and discussion

As shown in Fig. 1A, cancer cell populations inside a tumor or in the circulation system as circulating tumor cells (CTCs) show distinct stages of epithelial-mesenchymal transition (EMT) which corresponds to different levels of invasiveness for these cells. In order to decipher this invasiveness capacity, it is crucial to identify and categorize the cell population based on their heterogeneity in extracellular secretions (Gangoda et al., 2017; Ji et al., 2019); one of which is ECM-degrading enzyme matrix metalloproteinases (MMPs) (Köhrmann et al., 2009). To capture this heterogeneous response, here we introduce a capillary-assisted microfluidic single cell encapsulation technique which can maintain single cells in nanoliter droplets in long-term culture and provide a continuous data on single cell MMP secretion. The quantification of secretion is achieved through measuring the fluorescent signal proportional to the rate of reaction between the MMPs secreted by the encapsulated cells and the fluorogenic substrate. The substrate consists of a quenching component (Dabcyl acid) connected to a donor 5-FAM (5-Carboxyfluorescein) by an amino acid sequence Dabcyl-PChaGC (Me)HAK(5FAM)-NH2. Cleavage of the amino acid chain by the secreted MMP enzymes from a single cell reduces the quenching capability, leading to an increase in the fluorescent intensity in each nanoliter compartment (Bickett et al., 1993; Jing et al., 2015; Miller et al., 2011). As shown in Fig. 1B, the operation of this device is straightforward. First, the device PDMS slab is brought into conformal contact with a glass/TC surface and pressed gently to make a temporary seal. The cell sample is then injected into the device followed by blowing the middle

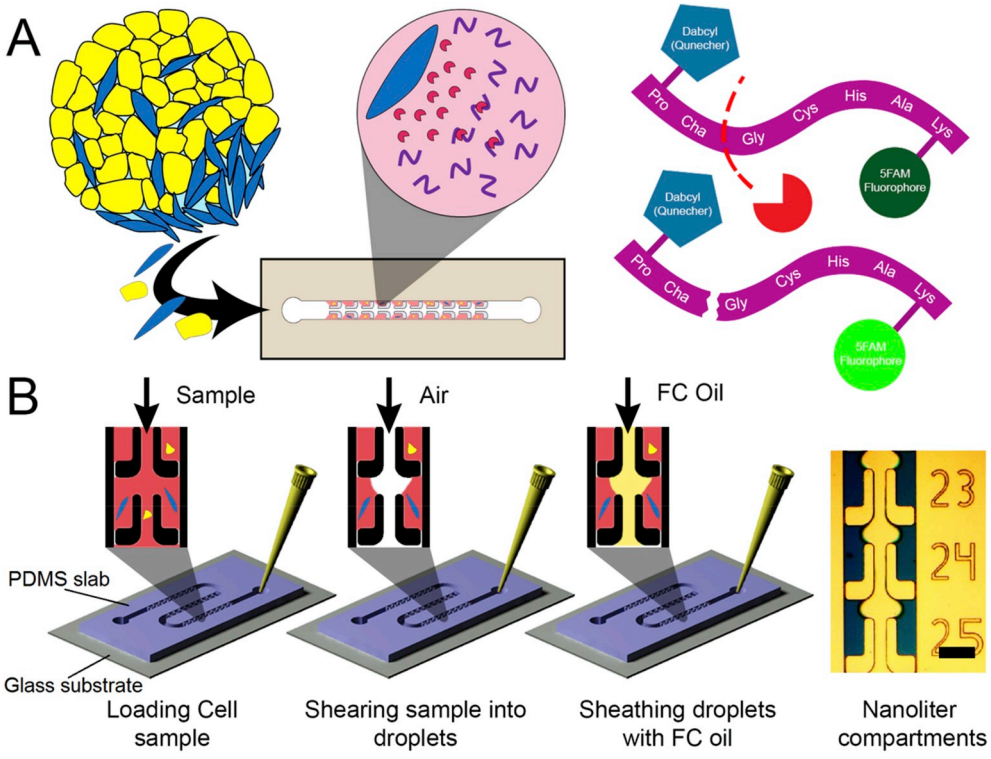

Fig. 1. Single cell encapsulation and real-time MMP secretion profiling; (A) Single cells from a heterogeneous cell population are loaded into a microfluidic device for single cell encapsulation; Biosensing of single cell MMP secretion is achieved by measuring the increase in fluorescent signal of a probe activated by cleavage of amino acid sequence. (B) Single cell encapsulation is achieved by capillary-stoppage of the liquid sample followed by shearing with air and sheathing with FC-40 oil. The nanoliter compartments filled with the blue food dye are shown in the right; Scale bar: 100 μm. (For interpretation of the references to color in this figure legend, the reader is referred to the Web version of this article.)

channel with air to remove residual sample and addition of Fluorinert™ FC-40 fluorocarbon oil (3M, USA) to sheath the droplets. Each of the nanoliter compartments is surrounded by the trap walls, and is separated from the adjacent compartment via a 10 μm width air plug. The device and each traps dimensions are provided in Fig. S3. The technique presented here does not rely on surface functionalization, and facilitates the single cell functional analysis by easier capture of single cells as well as eliminating the need for surface-bound immunoassays.

3.1. Capillary-assisted formation of nanoliter compartments

Successful formation of nanoliter compartments in our approach depends on the controlled movement of liquid-gas interface which is adjusted by the geometry of the channel. To understand this effect, here we present an analysis of the physics of this flow and the effect of capillary and flow resistive forces by tracking the liquid front along the channel. Fig. 2A demonstrates the geometry of the device. As can be seen the capillary forces act against the filling pressure forcing the interface to take a convex shape.

Capillary-assisted liquid manipulation takes place under three functions; stoppage (region 1 in Fig. 2A), deceleration (region 2) and acceleration (regions 3 and 4) of the liquid-gas interface (shown in green line). When the interface reaches the narrow end of a trap (region 1), the capillary pressure builds up significantly, pushes back the interface and finally stabilizes the position of the contact point. In the middle of the channel (region 2), a slight contraction ratio is designed which decelerates the interface movement and gives the liquid sample enough time to fill the trap. In designing the geometry of each trap, divergent channel walls were designed to accelerate the liquid movement which is confirmed by looking at the rate of change in the contact point position in region 3. In addition, the width of trap's entrance ($w_{ent.} = 100$ μm) was designed to be bigger than the channel width ($w_{channel} = 70$ μm) to prevent trapping of air bubble in the system. Finally, an expansion area is designed to accelerate the flow from the narrow middle channel to the next pair of traps (region 4).

Fig. 2B demonstrates the evolution of the interface movement as well as the pressure distribution in the device. Looking into the pressure distribution, it is evident that the pressure at the liquid side initially reduces as the interface passes through a gradual expansion (from $t = 6 \times 10^{-3}$s to 1.2×10^{-3}s). This decrease continues up to $t = 1.8 \times 10^{-3}$s at which the interface faces the entrance to the traps and the narrow middle channel. From this point, the capillary pressure increases which subsequently demand a higher filling pressure. This behavior can also be seen by looking into the distribution of the velocity vector (Fig. S4). From $t = 6 \times 10^{-3}$s up to $t = 2.3 \times 10^{-3}$s at which the liquid-air interface makes contact with the trifurcation, the velocity magnitude increases.

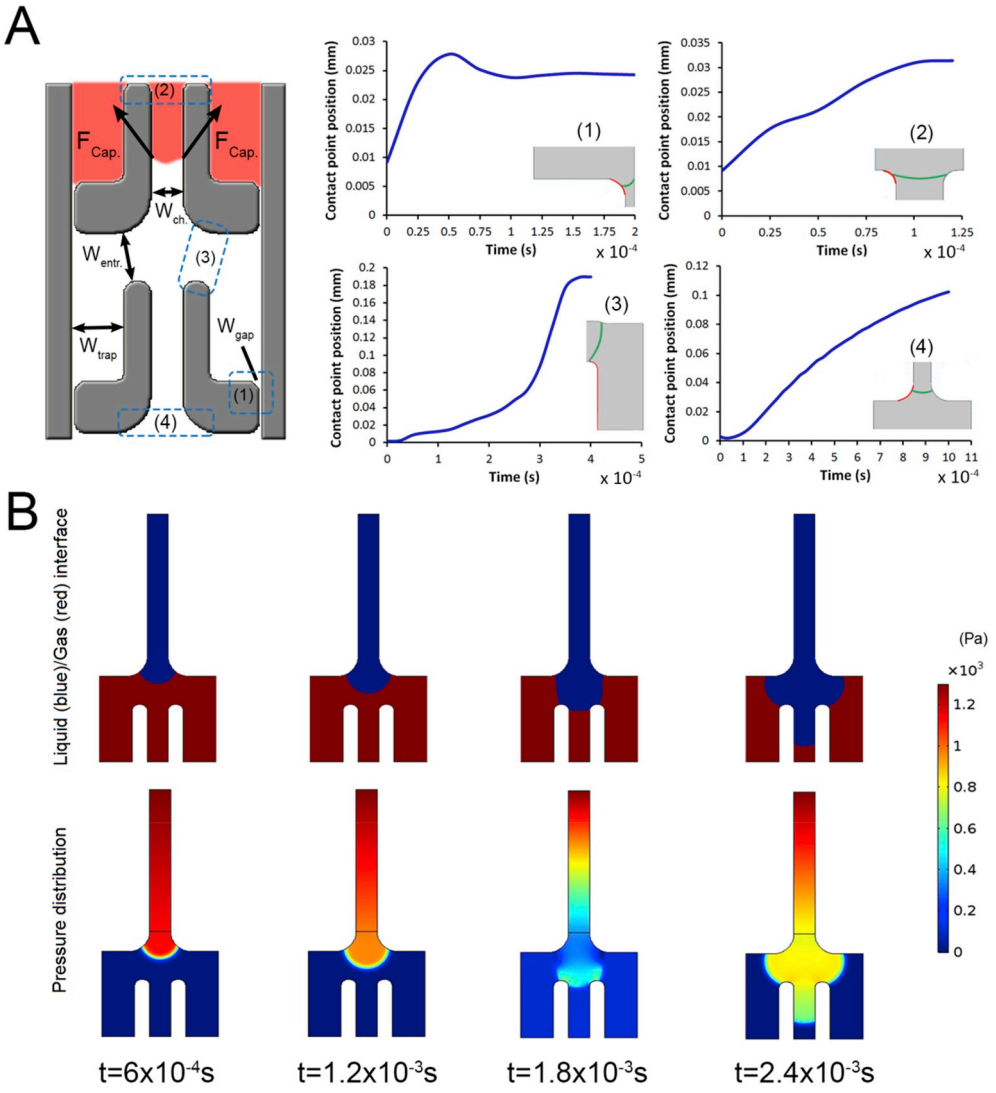

Fig. 2. The operational analysis of the device by analyzing the fluid flow; (A) Geometrical variations lead to liquid-gas interface stoppage, deceleration and acceleration in different regions of the device's design. (B) Evolution of the liquid-gas interface movement as well as pressure distribution during device filling step.

After this time the velocity further increases at the trap sides (at t = 2.5 × 10^{-3}s) which pushes the liquid to fill the traps.

3.2. Single cell encapsulation in nanoliter compartments

As shown in Fig. 3A, following sample injection and droplet formation in the microfluidic device, each compartment contains a different number of cells. A desirable encapsulation scenario for cell secretion profiling is the one which gives the maximum number of compartments with only a single cell. In addition, compartments with two cells can be used for studying the effects of single cell secretion for cell-to-cell communication. Two trap sizes of 2.5 nl and 14 nl were

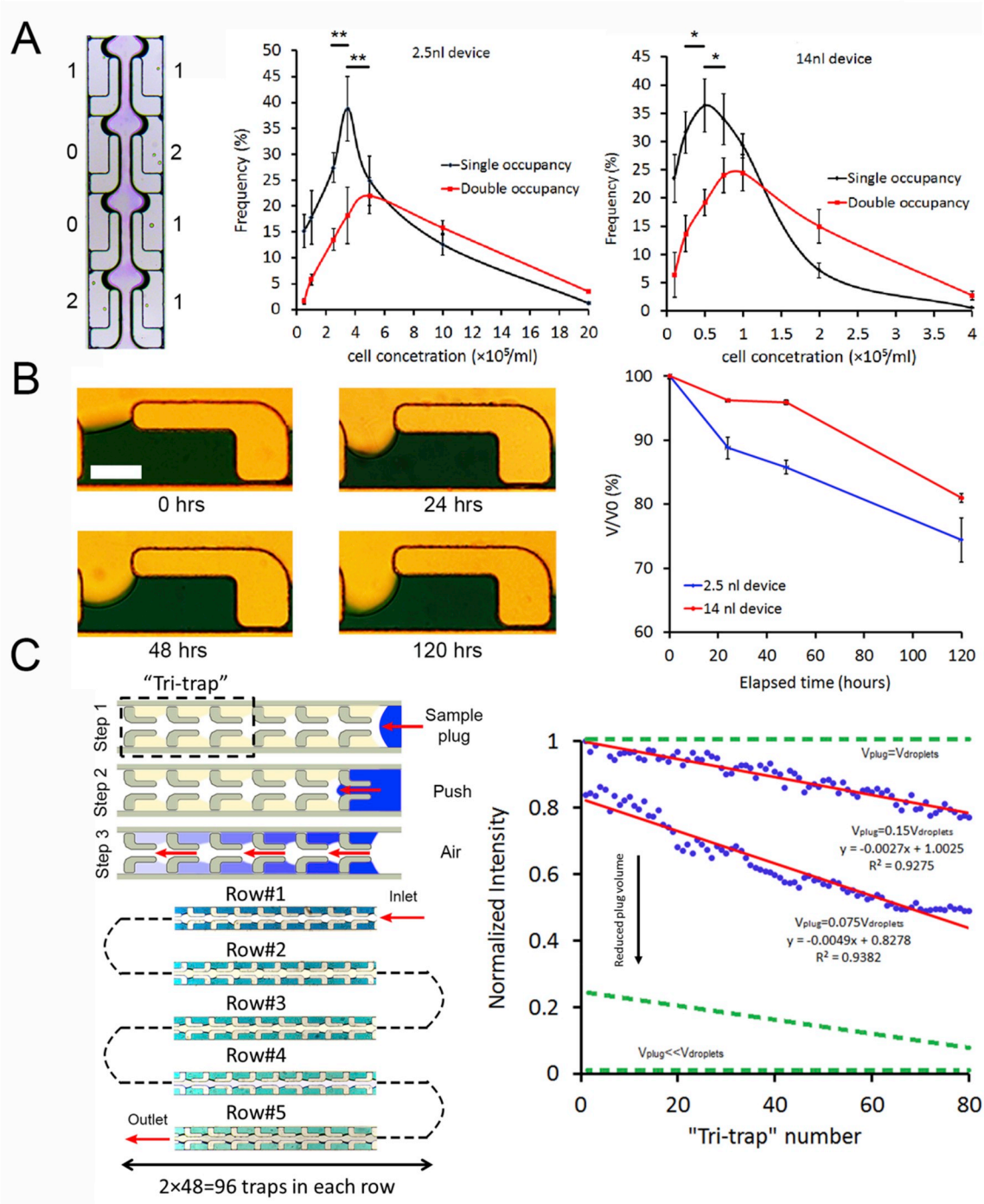

Fig. 3. Characterization and encapsulation efficiency of the nanoliter compartments: (A) Cell occupancy in nanoliter compartments with two different trapping size and the optimal concentration for achieving single and double cell occupancy which is 3.5 × 105/ml (at 38.8% of the traps) and 5 × 105/ml (at 21.9% of the traps) for 2.5 nl device and 0.5 × 105/ml (at 36.4% of the traps) and 1 × 105/ml (at 24.4% of the traps) for 14 nl device, (n = 10; presented data is mean ± SD) (B) Size-dependent droplet evaporation, for 2.5 nl device, 85% and 74% of the initial droplet volume were maintained after 48 and 120 h while for 14 nl device these numbers were 96% and 81% respectively (n = 3; presented data is mean ± SD); Scale bar: 100 μm. (C) Manipulation of droplet composition and generation of gradient of chemical factors by adding a plug of chemical (n = 3). By adjusting the plug volume, gradients of different steepness can be achieved; The bigger plug volume will lead to a less steep gradient. An asymptotic condition is when the plug is big enough leading to a horizontal line of zero gradient in the array which is equal to droplet dilution.

designed to accommodate a variety of cells. The bigger trap size (14 nl) were especially designed for trapping larger cells, spheroids, and particles as well as providing space for single cell proliferation/medium depletion in sensitive cells. In order to maximize the possibility of these events, the cell sample concentration needs to be adjusted. For instance, for the device with 2.5 nl compartments, cell sample concentrations of 3.5×10^5/ml and 5×10^5/ml provide maximum single (=38.8%) and maximum double occupancy (=21.9%) respectively (Fig. 3A). For the device with a bigger 14 nl compartments, these numbers do not show a significant difference (36.4% and 24.4% for single and double occupancy respectively) as cell occupancy follows the Poisson distribution. However, since the compartments are bigger, the cell sample concentrations are decreased to 0.5×10^5/ml and 1×10^5/ml respectively.

Although achieving nanoliter volumes is a requirement for single cell encapsulation, the small size of the liquid compartments makes it prone to extensive evaporation. In order to reduce evaporation after the droplet formation, the middle channel was filled with FC-40 oil, the inlet and outlet ports were covered with adhesive tape and the device was

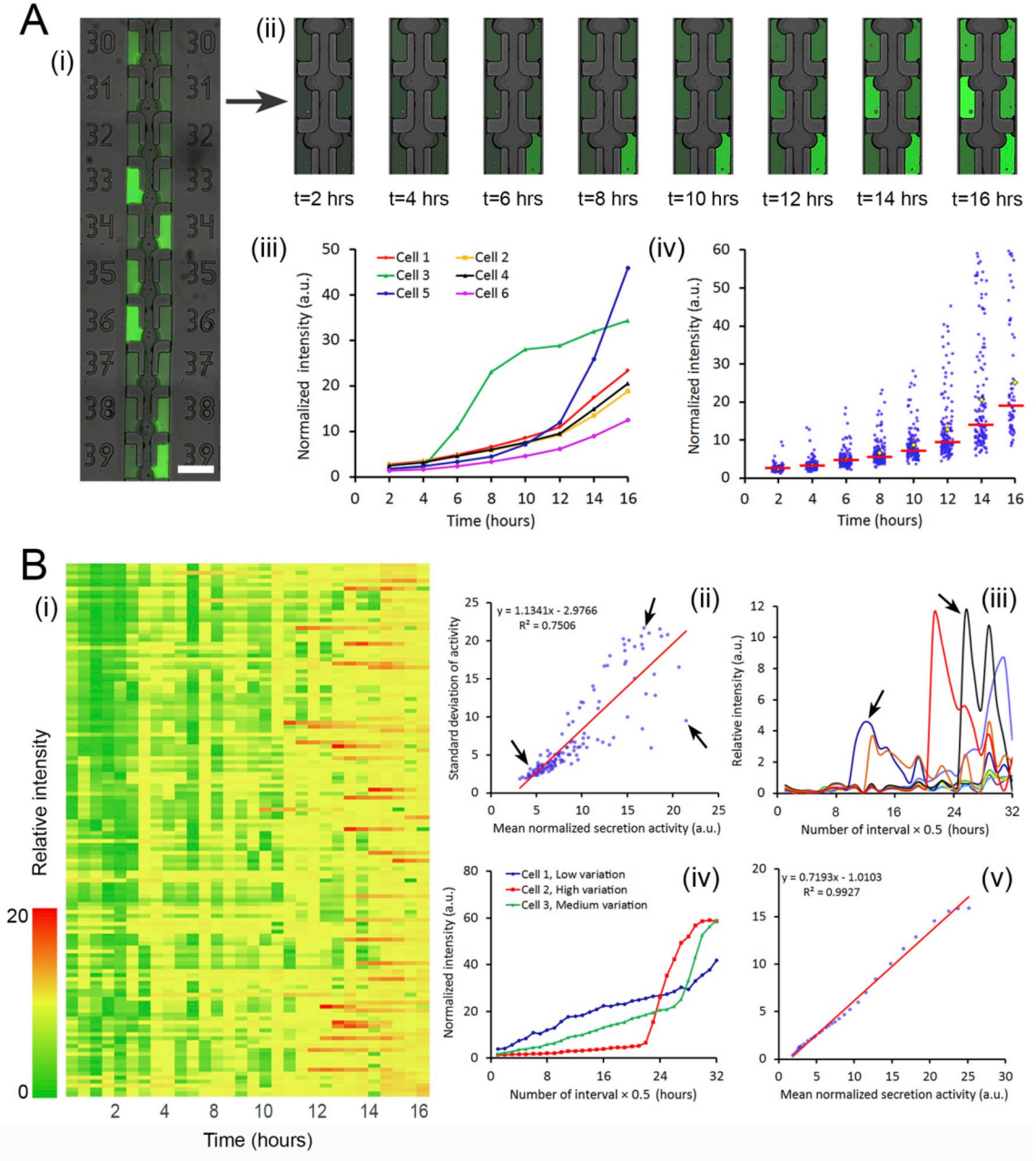

Fig. 4. Single cell secretion dynamics profiling: (A) Spatiotemporal analysis of the secretion activity of the single cell population, (i) An image demonstrating the on chip measurement of the MMP secretion activity of an array of isolated single breast cancer cells at a certain time point, (ii) evolution of single cell secretion activity over time, (iii) The corresponding change in fluorescent activity of the representative cells over time: each cell shows a unique secretion dynamics, (iv) Secretion dynamics of the whole single cell population over time, the average secretion of cells show significant increase over time ($p < 0.05$). (B) Single cell resolution secretion analysis: (i) Heat map presenting the heterogeneous secretion levels of single cells at equal 0.5 h intervals over the course of the experiment (N = 135), (ii) Different modes of dynamic MMP secretion in the single cell population; The mean and standard deviation of MMP activity of MDA-MB-231 cells. Red line shows the regression of the correlation between average and standard deviation. (iii) Single cell with extreme activity versus single cells with gradual and slow variations, (iv) representative cells from each secretion type, (v) variation in the secretion of the population over time showing a steady trend; Scale bar: 300 μm. (For interpretation of the references to color in this figure legend, the reader is referred to the Web version of this article.)

placed in a saturated petri dish chamber. With these precautions, the droplet volume in the 2.5 nl device could be maintained at 85% and 74% of the initial droplet after 48 and 120 h, respectively (Fig. 3B). For the device with 14 nl trap, evaporation occurred at lower rate and 96% and 81% of the droplet volume was maintained after 48 and 120 h respectively.

Given the capability of generating hundreds of nanoliter compartments, we further investigated the possibility of manipulating their composition. This manipulation can be used for adding fresh media to the cells to extend their viability, and in generating a gradient of a biological factor (e.g. growth factors, antibiotics, etc) in the array of compartments for high throughput dose dependent single cell response. To demonstrate this capability, a certain volume (a plug) of the sample (shown in blue color in Fig. 3C) was injected in the device and pushed to move along the channels. Mass exchange between the plug and each compartment occurs when the plug is in contact with the compartment. As shown in Fig. 3C, this leads to formation of a linear gradient of the blue food dye along the length of the droplet array. The steepness of this gradient can be controlled by adjusting the volume of the plug (The steepness plots in Fig. 3C). Longer plugs with higher volume can be used for generating mild gradients while shorter plugs with lower volume can be used to generate steeper gradients.

3.3. Single cell secretion dynamics profiling

Having the capability of maintaining single cells in isolated compartments over a long period of time enables measuring their secretion dynamics. The secreted molecules from individual cells are preserved within each nanoliter compartment and their level is quantified using a biochemical sensing reaction. In this paper, our aim was to reveal the MMP secretion dynamics heterogeneity among single breast cancer cells. This was achieved by measuring the fluorescent intensity of fluorophore 5FAM which is activated as a product of substrate cleavage by the secreted MMP molecules (Fig. 1A). Before performing the MMP assay, single cells' on-chip viability was measured and viability of >90% was ensured over the 16 h of the experiment (Fig. S5, Method S1).

Fig. 4A(i) demonstrates the on chip measurement of the MMP secretion activity of an array of isolated single breast cancer cells at a certain time point. Since MMP activity is proportional to the fluorophore activation, droplets containing active single cells fluoresce more than those with less active cells. In addition, droplets lacking cells showed no change in fluorescent activity in the control experiments (see Fig. S6), confirming that change in fluorescence is solely relied on MMP secretion from the cells. By scanning the chip in a matter of less than a minute, and stitching the obtained images together, a bird eye view of the whole array was achieved which provides a visual picture of the secretion heterogeneity among the population. This capability is enabled by adjusting the compartment density through a symmetrical chip design (Fig. S3). Fig. 4A(ii) presents our method's capability to capture the evolution of single cell's secretion activity over time. Since cells are encapsulated in geometrically fixed droplets, their dynamic secretion activity can be watched by locating the exact droplet coordinates or by looking at their associated numeric index. As shown here, each cell shows a unique secretion dynamics which is depicted by their associated change in fluorescent intensity. The fluorescent intensity is quantified in Fig. 4A(iii); Although all cells initially show similar fluorescent levels, cell 3 shows an early spike in its activity leading to an augmented secretion levels compared to the rest of the population. In addition, cell 5 initially shows similar activity compared to the other cells but later deviates from them with a sharp increase in its activity at 12 h. Therefore, cell 3 and cell 5 are more aggressive compared to the other four cells.

In order to study the MMP activity of the whole population, the fluorescent intensity of all compartments containing single cells were achieved and presented in Fig. 4A(iv). As can be seen here, the average protease activity of the population shows an accelerating trend. Therefore, it can be inferred that the population becomes more aggressive over time. In addition, since the average value of the activities deviates from the median, it can be concluded that the population has a heterogeneous activity with more cells leaning toward higher activity over time. Table S1, presents a comparison of the average MMP secretion activity of MDA-MB-231 in the presented system with the previous methods, verifying the similar trends in average cells response over time regardless of the method used.

While looking into the response of the population can provide an overview of the cells' secretion dynamics, a deeper analysis is required to understand the role of each cell in the population. In order to achieve single cell resolution analysis, we measured the variation in protease activity of each cell in every 30 min interval during the 16 h experimental timeframe. Fig. 4B(i) presents the heat map of single cell's activity in these intervals in which a wide variety of secretion dynamics can be observed. To harness a pattern and identify the most aggressive subpopulations, the mean and standard deviation of the cells secretion dynamics were calculated based on their activity on the heat map. As can be seen from the scatterplot of Fig. 4B(ii), different modes of secretion dynamics can be found. The first mode is a group of single cells that secrete slowly and with a quite low variation in their secretion dynamics (the data located below the red CV line). On the contrary, the second mode shows a high level of variation with sharp spikes in activity (the data above the red CV line). As shown in Fig. 4B (iii), these spikes can be mild and happen at the early stage of culture or can be intense and take place at the end of the culture period. Another mode of response is a subpopulation with a variation between the first two modes located on the CV line. Interestingly, most of the cells in the population are showing this mode of secretion as can be inferred from the high density of data points overlapping the CV line. A notable feature of these cells is their low average secretion over the experimental timeframe. This means that the most aggressive subpopulation are among a small number of cells on the two ends of the secretion dynamics, i.e. cells with high and gradual secretion and cells with spikes in secretion. An example of a cell in each of those modes of response is presented in Fig. 4B(iv). Finally, we measured the variation of the secretion dynamics of the whole population over the course of the experiment (Fig. 4v). It is found that although cells behave differently when compared together, the secretion activity of the population remains steady and with low variation over time.

4. Conclusions

The ability to capture the heterogeneous MMP secretion dynamics among single cancer cells provides valuable information regarding their interaction with their surrounding tissue and the role of individual cells in tumor metastasis (Cathcart et al., 2015). Such information can be very useful in the development of therapeutic drugs targeting these biomolecules. To enable single cell level secretion measurements, we report a new capillary-assisted microfluidic biosensing approach which is based on a rapid encapsulation of single cancer cells in nanoliter compartments. We present for the first time the two phase fluid mechanics and capillary forces underpinning the simultaneous formation and splitting of droplet compartments and discuss the underlying mechanism governing the air venting in such systems. Our analysis explains how the geometry of the microfluidic system affects successful droplet formation by adjusting the sample movement based on the geometry-dependent capillary pressure. In order to assess the functionality of the presented approach for single cell secretion assays, critical parameters such as single cell encapsulation efficiency of 38.8%, droplet volume evaporation rate of 10% in 48 h and manipulation of droplet composition through controlled gradient generation were studied. Single cell secretion dynamics in nanoliter dynamics were quantified through a FRET-based biosensing assay which produces fluorescent signal upon substrate cleavage. The results showed that while the average single cancer cell population becomes more active over time,

each single cell has its unique secretion history. Measurement of single cell secretion in discrete intervals revealed a variety of dynamics secretion modes. It was found that most cells in the population possess low secretion levels. However, cells with secretion dynamics that include sharp spikes or slow but progressive trend are more aggressive as indicated by their higher average secretion. The microfluidic approach presented here is rapid to implement, needs no engineering expertise, and is effective in measuring single cell dynamic behavior over time. Compared to the droplet-based microfluidic systems, the presented method is much simpler to perform, enables tracking multiple immobilized single cells, and support culture of adherent cells. One limitation of the method is the fixed number of traps dictated by the design. However, for the studies requiring thousands of cells either multiple devices can be used or the number of traps can be decided before device design and fabrication.

Author contributions

The manuscript was written through contributions of all authors. All authors have given approval to the final version of the manuscript.

Declaration of competing interest

The authors declare that they have no known competing financial interests or personal relationships that could have appeared to influence the work reported in this paper.

CRediT authorship contribution statement

Amin Hassanzadeh-Barforoushi: Conceptualization, Investigation, Methodology, Validation, Funding acquisition, Visualization, Data curation, Writing - original draft, Writing - review & editing. **Majid Ebrahimi Warkiani:** Conceptualization, Resources, Methodology, Writing - review & editing. **David Gallego-Ortega:** Supervision, Resources, Writing - review & editing. **Guozhen Liu:** Resources, Writing - review & editing. **Tracie Barber:** Supervision, Resources, Writing - review & editing.

Acknowledgements

A. H–B. would like to acknowledge the funding through the post-doctoral writing fellowship scheme provided by the faculty of Engineering, University of New South Wales (UNSW). G. Liu acknowledges the funding support of the ARC Future Fellowship (FT160100039). We would like to thank Garvan Institute of Medical Research/the Kinghorn Cancer Centre for kindly providing the cancer cell lines for this research.

Appendix A. Supplementary data

Supplementary data to this article can be found online at https://doi.org/10.1016/j.bios.2020.112113.

References

Amantonico, A., Urban, P.L., Fagerer, S.R., Balabin, R.M., Zenobi, R., 2010. Single-cell MALDI-MS as an analytical tool for studying intrapopulation metabolic heterogeneity of unicellular organisms. Anal. Chem. 82, 7394–7400. https://doi.org/10.1021/ac1015326.

Atkin-Smith, G.K., Paone, S., Zanker, D.J., Duan, M., Phan, T.K., Chen, W., Hulett, M.D., Poon, I.K.H., 2017. Isolation of cell type-specific apoptotic bodies by fluorescence-activated cell sorting. Sci. Rep. 7, 39846.

Bickett, D.M., Green, M.D., Berman, J., Dezube, M., Howe, A.S., Brown, P.J., Roth, J.T., Mcgeehan, G.M., 1993. A high throughput fluorogenic substrate for interstitial collagenase (MMP-1) and gelatinase (MMP-9). Anal. Biochem. 212, 58–64. https://doi.org/10.1006/abio.1993.1291.

Cao, C., Zhang, F., Goldys, E.M., Gao, F., Liu, G., 2018. Advances in structure-switching aptasensing towards real time detection of cytokines. Trac. Trends Anal. Chem. 102, 379–396. https://doi.org/10.1016/j.trac.2018.03.002.

Cathcart, J., Pulkoski-Gross, A., Cao, J., 2015. Targeting matrix metalloproteinases in cancer: bringing new life to old ideas. Genes & Diseases 2, 26–34. https://doi.org/10.1016/j.gendis.2014.12.002.

Chen, Z., Lu, Y., Zhang, K., Xiao, Y., Lu, J., Fan, R., 2019. Multiplexed, sequential secretion analysis of the same single cells reveals distinct effector response dynamics dependent on the initial basal state. Adv. Sci. 6 https://doi.org/10.1002/advs.201801361, 1801361.

Chokkalingam, V., Tel, J., Wimmers, F., Liu, X., Semenov, S., Thiele, J., Figdor, C.G., Huck, W.T.S., 2013. Probing cellular heterogeneity in cytokine-secreting immune cells using droplet-based microfluidics. Lab Chip 13, 4740–4744. https://doi.org/10.1039/C3LC50945A.

Cohen, D.E., Schneider, T., Wang, M., Chiu, D.T., 2010. Self-digitization of sample volumes. Anal. Chem. 82, 5707–5717. https://doi.org/10.1021/ac100713u.

Collins, D.J., Neild, A., deMello, A., Liu, A.-Q., Ai, Y., 2015. The Poisson distribution and beyond: methods for microfluidic droplet production and single cell encapsulation. Lab Chip 15, 3439–3459. https://doi.org/10.1039/C5LC00614G.

Colombo, S., Broggi, S., Collini, M., D'Alfonso, L., Chirico, G., Martegani, E., 2017. Detection of cAMP and of PKA activity in Saccharomyces cerevisiae single cells using Fluorescence Resonance Energy Transfer (FRET) probes. Biochem. Biophys. Res. Commun. 487, 594–599. https://doi.org/10.1016/j.bbrc.2017.04.097.

Courtney, M., Chen, X., Chan, S., Mohamed, T., Rao, P.P.N., Ren, C.L., 2017. Droplet microfluidic system with on-demand trapping and releasing of droplet for drug screening applications. Anal. Chem. 89, 910–915. https://doi.org/10.1021/acs.analchem.6b04039.

Dang, B.V., Hassanzadeh-Barforoushi, A., Syed, M., Yang, D., Kim, S.-J., Taylor, R.A., Liu, G.-J., Liu, G., Barber, T., 2019. Microfluidic actuation via 3D-printed molds towards multiplex biosensing of cell apoptosis. ACS Sens. https://doi.org/10.1021/acssensors.9b01057.

Dhar, M., Lam, J.N., Walser, T., Dubinett, S.M., Rettig, M.B., Carlo, D.D., 2018. Functional profiling of circulating tumor cells with an integrated vortex capture and single-cell protease activity assay. Proc. Natl. Acad. Sci. Unit. States Am. 115, 9986–9991. https://doi.org/10.1073/pnas.1803884115.

Eyer, K., Kuhn, P., Hanke, C., Dittrich, P.S., 2012. A microchamber array for single cell isolation and analysis of intracellular biomolecules. Lab Chip 12, 765–772. https://doi.org/10.1039/C2LC20876H.

Gangoda, L., Liem, M., Ang, C.-S., Keerthikumar, S., Adda, C.G., Parker, B.S., Mathivanan, S., 2017. Proteomic profiling of exosomes secreted by breast cancer cells with varying metastatic potential. Proteomics 17. https://doi.org/10.1002/pmic.201600370, 1600370.

Haaß, W., Kleiner, H., Müller, M.C., Hofmann, W.-K., Fabarius, A., Seifarth, W., 2015. Measurement of separase proteolytic activity in single living cells by a fluorogenic flow cytometry assay. PloS One 10, e0133769. https://doi.org/10.1371/journal.pone.0133769.

Han, Q., Bradshaw, E.M., Nilsson, B., Hafler, D.A., Love, J.C., 2010. Multidimensional analysis of the frequencies and rates of cytokine secretion from single cells by quantitative microengraving. Lab Chip 10, 1391–1400. https://doi.org/10.1039/B926849A.

Hassanzadeh-Barforoushi, A., Shemesh, J., Farbehi, N., Asadnia, M., Yeoh, G.H., Harvey, R.P., Nordon, R.E., Warkiani, M.E., 2016. A rapid co-culture stamping device for studying intercellular communication. Sci. Rep. 6, 35618. https://doi.org/10.1038/srep35618.

Hassanzadeh-Barforoushi, A., Law, A.M.K., Hejri, A., Asadnia, M., Ormandy, J., C, Gallego-Ortega, D., Warkiani, M.E., 2018. Static droplet array for culturing single live adherent cells in an isolated chemical microenvironment. Lab Chip 18, 2156–2166. https://doi.org/10.1039/C8LC00403J.

Ismail, A.E., Grest, G.S., Heine, D.R., Stevens, M.J., Tsige, M., 2009. Interfacial structure and dynamics of siloxane systems: PDMS−Vapor and PDMS−Water. Macromolecules 42, 3186–3194. https://doi.org/10.1021/ma802805y.

Jeknić, S., Kudo, T., Covert, M.W., 2019. Techniques for studying decoding of single cell dynamics. Front. Immunol. 10 https://doi.org/10.3389/fimmu.2019.00755.

Ji, Y., Qi, D., Li, L., Su, H., Li, X., Luo, Y., Sun, B., Zhang, F., Lin, B., Liu, T., Lu, Y., 2019. Multiplexed profiling of single-cell extracellular vesicles secretion. Proc. Natl. Acad. Sci. Unit. States Am. 116, 5979–5984. https://doi.org/10.1073/pnas.1814348116.

Jing, T., Ramji, R., Warkiani, M.E., Han, J., Lim, C.T., Chen, C.-H., 2015. Jetting microfluidics with size-sorting capability for single-cell protease detection. Biosens. Bioelectron. 66, 19–23. https://doi.org/10.1016/j.bios.2014.11.001.

Köhrmann, A., Kammerer, U., Kapp, M., Dietl, J., Anacker, J., 2009. Expression of matrix metalloproteinases (MMPs) in primary human breast cancer and breast cancer cell lines: new findings and review of the literature. BMC Canc. 9, 188. https://doi.org/10.1186/1471-2407-9-188.

Konry, T., Dominguez-Villar, M., Baecher-Allan, C., Hafler, D.A., Yarmush, MartinL., 2011. Droplet-based microfluidic platforms for single T cell secretion analysis of IL-10 cytokine. Biosens. Bioelectron. 26, 2707–2710. https://doi.org/10.1016/j.bios.2010.09.006.

Konry, T., Sarkar, S., Sabhachandani, P., Cohen, N., 2016. Innovative tools and technology for analysis of single cells and cell–cell interaction. Annu. Rev. Biomed. Eng. 18, 259–284. https://doi.org/10.1146/annurev-bioeng-090215-112735.

Köster, S., Angilè, F.E., Duan, H., Agresti, J.J., Wintner, A., Schmitz, C., Rowat, A.C., Merten, C.A., Pisignano, D., Griffiths, A.D., Weitz, D.A., 2008. Drop-based microfluidic devices for encapsulation of single cells. Lab Chip 8, 1110–1115. https://doi.org/10.1039/B802941E.

Krieger, T., Simons, B.D., 2015. Dynamic stem cell heterogeneity. Development 142, 1396. https://doi.org/10.1242/dev.101063.

Li, X., Soler, M., Szydzik, C., Khoshmanesh, K., Schmidt, J., Coukos, G., Mitchell, A., Altug, H., 2018. Label-free optofluidic nanobiosensor enables real-time analysis of

single-cell cytokine secretion. Small 14, 1800698. https://doi.org/10.1002/smll.201800698.

Li, Q., Li, W., Cui, S., Sun, Q., Si, H., Chen, Z., Xu, K., Li, L., Tang, B., 2019. Dynamic fluorescent imaging analysis of mitochondrial redox in single cells with a microfluidic device. Biosens. Bioelectron. 129, 132–138. https://doi.org/10.1016/j.bios.2019.01.005.

Liu, G., Bursill, C., Cartland, S.P., Anwer, A.G., Parker, L.M., Zhang, K., Feng, S., He, M., Inglis, D.W., Kavurma, M.M., Hutchinson, M.R., Goldys, E.M., 2019. A nanoparticle-based affinity sensor that identifies and selects highly cytokine-secreting cells. iScience 20, 137–147. https://doi.org/10.1016/j.isci.2019.09.019.

Lo, C.-A., Kays, I., Emran, F., Lin, T.-J., Cvetkovska, V., Chen, B.E., 2015. Quantification of protein levels in single living cells. Cell Rep. 13, 2634–2644. https://doi.org/10.1016/j.celrep.2015.11.048.

Macosko, E.Z., Basu, A., Satija, R., Nemesh, J., Shekhar, K., Goldman, M., Tirosh, I., Bialas, A.R., Kamitaki, N., Martersteck, E.M., Trombetta, J.J., Weitz, D.A., Sanes, J. R., Shalek, A.K., Regev, A., McCarroll, S.A., 2015. Highly parallel genome-wide expression profiling of individual cells using nanoliter droplets. Cell 161, 1202–1214. https://doi.org/10.1016/j.cell.2015.05.002.

Miller, M.A., Barkal, L., Jeng, K., Herrlich, A., Moss, M., Griffith, L.G., Lauffenburger, D. A., 2011. Proteolytic Activity Matrix Analysis (PrAMA) for simultaneous determination of multiple protease activities. Int Bio (Cam) 3, 422–438. https://doi.org/10.1039/c0ib00083c.

Nejat, A., Kowsary, F., Hasanzadeh-Barforoushi, A., Ebrahimi, S., 2014. Unsteady pulsating characteristics of the fluid flow through a sudden expansion microvalve. Microfluid. Nanofluidics 17, 623–637. https://doi.org/10.1007/s10404-014-1343-9.

Pickrell, J.K., Marioni, J.C., Pai, A.A., Degner, J.F., Engelhardt, B.E., Nkadori, E., Veyrieras, J.-B., Stephens, M., Gilad, Y., Pritchard, J.K., 2010. Understanding mechanisms underlying human gene expression variation with RNA sequencing. Nature 464, 768.

Rafeie, M., Welleweerd, M., Hassanzadeh-Barforoushi, A., Asadnia, M., Olthuis, W., Ebrahimi Warkiani, M., 2017. An easily fabricated three-dimensional threaded lemniscate-shaped micromixer for a wide range of flow rates. Biomicrofluidics 11, 014108. https://doi.org/10.1063/1.4974904.

Satija, R., Shalek, A.K., 2014. Heterogeneity in immune responses: from populations to single cells. Trends. Immunol., Gene Expr. Immune Syst. 35, 219–229. https://doi.org/10.1016/j.it.2014.03.004.

Shemesh, J., Arye, T.B., Avesar, J., Kang, J.H., Fine, A., Super, M., Meller, A., Ingber, D. E., Levenberg, S., 2014. Stationary nanoliter droplet array with a substrate of choice for single adherent/nonadherent cell incubation and analysis. Proc. Natl. Acad. Sci. Unit. States Am. 111, 11293–11298. https://doi.org/10.1073/pnas.1404472111.

Shen, F.-M., Zhu, L., Ye, H., Yang, Y.-J., Pang, D.-W., Zhang, Z.-L., 2015. A high throughput micro-chamber array device for single cell clonal cultivation and tumor heterogeneity analysis. Sci. Rep. 5, 11937.

Shendure, J., Balasubramanian, S., Church, G.M., Gilbert, W., Rogers, J., Schloss, J.A., Waterston, R.H., 2017. DNA sequencing at 40: past, present and future. Nature 550, 345.

Shirasaki, Y., Yamagishi, M., Suzuki, N., Izawa, K., Nakahara, A., Mizuno, J., Shoji, S., Heike, T., Harada, Y., Nishikomori, R., Ohara, O., 2014. Real-time single-cell imaging of protein secretion. Sci. Rep. 4, 4736.

Sposito, A.J., DeVoe, D.L., 2017. Staggered trap arrays for robust microfluidic sample digitization. Lab Chip 17, 4105–4112. https://doi.org/10.1039/C7LC00846E.

Stefen, H., Hassanzadeh-Barforoushi, A., Brettle, M., Fok, S., Suchowerska, A.K., Tedla, N., Barber, T., Warkiani, M.E., Fath, T., 2018. A novel microfluidic device-based neurite outgrowth inhibition assay reveals the neurite outgrowth-promoting activity of tropomyosin Tpm3.1 in hippocampal neurons. Cell. Mol. Neurobiol. 38, 1557–1563. https://doi.org/10.1007/s10571-018-0620-7.

Stevens, M.M., Maire, C.L., Chou, N., Murakami, M.A., Knoff, D.S., Kikuchi, Y., Kimmerling, R.J., Liu, H., Haidar, S., Calistri, N.L., Cermak, N., Olcum, S., Cordero, N.A., Idbaih, A., Wen, P.Y., Weinstock, D.M., Ligon, K.L., Manalis, S.R., 2016. Drug sensitivity of single cancer cells is predicted by changes in mass accumulation rate. Nat. Biotechnol. 34, 1161–1167. https://doi.org/10.1038/nbt.3697.

Tay, S., Hughey, J.J., Lee, T.K., Lipniacki, T., Quake, S.R., Covert, M.W., 2010. Single-cell NF-κB dynamics reveal digital activation and analogue information processing. Nature 466, 267–271. https://doi.org/10.1038/nature09145.

Vitak, S.A., Torkenczy, K.A., Rosenkrantz, J.L., Fields, A.J., Christiansen, L., Wong, M.H., Carbone, L., Steemers, F.J., Adey, A., 2017. Sequencing thousands of single-cell genomes with combinatorial indexing. Nat. Methods 14, 302.

Wu, M., Singh, A.K., 2012. Single-cell protein analysis. Curr. Opin. Biotechnol., Anal. Biotechnol. 23, 83–88. https://doi.org/10.1016/j.copbio.2011.11.023.

Zhang, F., Deng, F., Liu, G.-J., Middleton, R., Inglis, D.W., Anwer, A., Wang, S., Liu, G., 2019. IFN-γ-induced signal-on fluorescence aptasensors: from hybridization chain reaction amplification to 3D optical fiber sensing interface towards a deployable device for cytokine sensing. Mol. Syst. Des. Eng. 4, 872–881. https://doi.org/10.1039/C9ME00047J.

Zhou, Q., Kwa, T., Gao, Y., Liu, Y., Rahimian, A., Revzin, A., 2013. On-chip regeneration of aptasensors for monitoring cell secretion. Lab Chip 14, 276–279. https://doi.org/10.1039/C3LC50953B.